Rapid Communications

Intralayer ferromagnetism between $S = \frac{5}{2}$ ions in $MnBi_2Te_4$: Role of empty Bi *p* states

Jing Li,[1,2] J. Y. Ni,[1,2] X. Y. Li,[1,2] H.-J. Koo,[3] M.-H. Whangbo,[4,5] J. S. Feng,[1,6,*] and H. J. Xiang[1,2,†]

[1]*Department of Physics, Key Laboratory of Computational Physical Sciences (Ministry of Education), State Key Laboratory of Surface Physics, Fudan University, Shanghai 200433, People's Republic of China*

[2]*Collaborative Innovation Center of Advanced Microstructures, Nanjing 210093, People's Republic of China*

[3]*Department of Chemistry, Research Institute for Basic Sciences, Kyung Hee University, Seoul 02447, Korea*

[4]*Department of Chemistry, North Carolina State University, Raleigh, North Carolina 27695-8204, USA*

[5]*Group SDeng, State Key Laboratory of Structural Chemistry, Fujian Institute of Research on the Structure of Matter (FJIRSM), Chinese Academy of Sciences (CAS), Fuzhou 350002, China*

[6]*School of Physics and Materials Engineering, Hefei Normal University, Hefei 230601, People's Republic of China*

(Received 22 January 2020; accepted 28 April 2020; published 22 May 2020)

The layered magnetic topological insulator $MnBi_2Te_4$ is a promising platform to realize the quantum anomalous Hall effect because its layers possess intrinsic ferromagnetism. However, it is not well understood why the high-spin d^5 magnetic ions Mn^{2+} forming the Mn-Te-Mn spin exchange paths prefer ferromagnetic (FM) coupling, contrary to the prediction of the Goodenough-Kanamori rule that a TM-*L*-TM spin exchange where TM and *L* are a transition-metal magnetic cation and a main group ligand, respectively, is antiferromagnetic (AFM) even when the bond angle of the exchange path is 90°. Using density functional theory calculations, we show that the presence of Bi^{3+} ions is essential for the FM coupling in $MnBi_2Te_4$. Then, using a tight-binding model Hamiltonian, we find that high-spin d^5 ions ($S = 5/2$) in TM-*L*-TM spin exchange paths prefer FM coupling if the empty *p* orbitals of a nonmagnetic cation *M* (e.g., Bi^{3+} ion) hybridize strongly with those of the bridging ligand *L* but AFM coupling otherwise.

DOI: 10.1103/PhysRevB.101.201408

In the context of tremendous progress in topological materials [1,2], many attempts have been made to introduce magnetism in topological insulators (TIs) for emerging new physics and potential applications [3–8], which include the quantum anomalous Hall (QAH) effect and topological magnetoelectric effect. It is difficult to combine magnetism and topological properties in a natural insulator simultaneously. So far, there are two dominating methods of introducing magnetism, one is doping magnetic metal elements into TI [4,9,10], and the other is constructing a ferromagnet/TI heterostructure [11–15]. The former led to the experimental observation of the QAH effect at tens of millikelvin [10], and the latter has complicated technical requirements. Obviously, both are at the stage far from practical applications. Recently, the layered phase $MnBi_2Te_4$ was theoretically predicted to be an antiferromagnetic (AFM) TI [16,17] and was soon confirmed by experiments [18–20]. Each $MnBi_2Te_4$ layer has a seven-sheet structure with the stacking pattern of Te-Bi-Te-Mn-Te-Bi-Te [see Fig. 1(a)] where each sheet has a trigonal arrangement of atoms; the sheet of Mn and the two inner sheets of Te form a $MnTe_2$ layer. The latter is sandwiched between two sheets of Bi, and the resulting $MnTe_2Bi_2$ layer between two outer sheets of Te such that each Mn forms an $MnTe_6$ octahedron and each Bi is an $BiTe_6$ octahedron. The formal oxidation states of Mn, Bi, and Te are +2, +3, and −2, respectively, and each Mn^{2+} cation is in the high-spin state (d^5, $S = 5/2$). It is important to note that the inner Te atoms are the first-coordinate ligands of both Mn^{2+} and Bi^{3+} cations, namely, the inner Te^{2-} anions interact with both Mn^{2+} and Bi^{3+} cations through the Mn-Te-Bi bridges. The Mn^{2+} ions are ferromagnetically coupled in each $MnBi_2Te_4$ layer, so the topological property and magnetism of $MnBi_2Te_4$ depend on the number of $MnBi_2Te_4$ layers in a sample; $MnBi_2Te_4$ exhibits a topological axion state and antiferromagnetism in films containing an even number of layers but the QAH effect and ferromagnetism in films containing an odd number of layers [21–24]. Due to this layer-number-dependent magnetism, $MnBi_2Te_4$ is a multifunctional magnetic material with potential applications in two-dimensional magnetic materials [25,26]. Hence, it is important to study its magnetism from both a theoretical point of view and an application perspective.

Within each $MnTe_2$ layer of $MnBi_2Te_4$, the spin exchanges between adjacent Mn^{2+} ions are Mn-Te-Mn superexchanges. In predicting whether this type of spin exchange is FM or AFM, one often employs the Goodenough-Kanamori rule [27–31]. When the transition metal (TM) is a high-spin d^5 ion, the TM-ligand- (*L*-) TM spin exchange is predicted to be strongly AFM when the TM-*L*-TM bond angle is around 180° but weakly AFM when the bond angle is close to 90° [25]. Experimentally, the Mn-Te-Mn angle of $MnBi_2Te_4$ is 94.44° [32], so the intralayer ferromagnetism in $MnBi_2Te_4$ contradicts the well-known Goodenough-Kanamori rule. Oleś *et al.* [33] pointed out that the Goodenough-Kanamori rules may not be obeyed in transition-metal compounds with partially occupied t_{2g} orbitals (e.g., d^1 and d^2 electronic configurations) due to spin-orbital entanglement. In other words, it requires

*fjs@hfnu.edu.cn
†hxiang@fudan.edu.cn

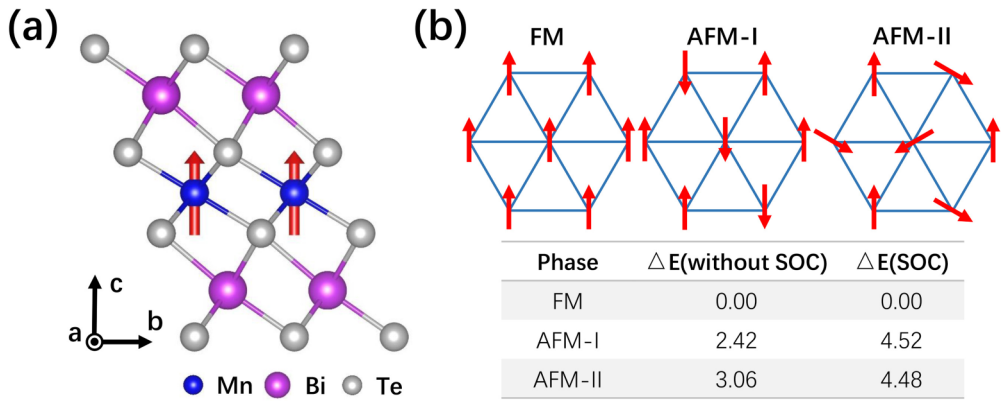

Phase	△E(without SOC)	△E(SOC)
FM	0.00	0.00
AFM-I	2.42	4.52
AFM-II	3.06	4.48

FIG. 1. (a) Side view of a $MnBi_2Te_4$ monolayer consisting of three sheets of cations and four sheets of anions. (b) The total energy of $MnBi_2Te_4$ in different magnetic states by setting the total energy of FM as a reference in units of meV/f.u. (where f.u. represents formula unit). The blue triangular lattice represents the Mn layer, and the red arrows represent the spin moments. There are three kinds of spin orders: FM (the upper left plane), AFM-I (AFM coupling between FM chains as shown in the upper center), and AFM-II (120° angle between any adjacent spin in the upper right plane). The lower panel of (b) lists the exchange energy without and with SOC for FM, AFM-I, and AFM-II.

the orbital degree of freedom to violate the Goodenough-Kanamori rules. However, this requirement is not met in $MnBi_2Te_4$ because both the majority-spin e_g and t_{2g} orbitals are fully occupied so that there is no orbital degree of freedom in $MnBi_2Te_4$.

In this Rapid Communication, we use first-principles density functional theory (DFT) calculations to verify the ferromagnetic (FM) coupling within a $MnBi_2Te_4$ layer and probe the microscopic origin of the intralayer FM coupling. We find that, for the FM coupling between the Mn^{2+} cations, the interactions of the Te^{2-} anion in each Mn-Te-Mn spin exchange path with its adjacent Bi^{3+} cation, which involves electron-density transfer from the Te^{2-} anion to the Bi^{3+} cation, are crucial. Furthermore, using a model Hamiltonian under the tight-binding approximation, we show why this is the case.

$MnBi_2Te_4$ is a van der Waals (vdW) material with space-group $R\bar{3}m$ for the bulk [32] and $P\bar{3}m1$ for the monolayer, and the weak vdW interactions between adjacent layers can hardly affect the intralayer magnetic interactions. Unless stated otherwise, we focus on a $MnBi_2Te_4$ monolayer throughout this Rapid Communication. The FM coupling between magnetic ions is also found in the layered phases $CrGeTe_3$ [25], CrI_3 [26], and Cr-doped systems [34] as well. However, the mechanism of FM coupling in $MnBi_2Te_4$ containing Mn^{2+} (d^5, $S = 5/2$) ions differs completely from that in CrI_3 and $CrGeTe_3$, which are made up of CrI_6 octahedra containing Cr^{3+} (d^3, $S = 3/2$) ions; in CrI_3 and $CrGeTe_3$, the e_g state of each CrI_6 octahedron is empty whereas, in $MnBi_2Te_4$, both the t_{2g} and the e_g states of each $MnTe_6$ octahedron are occupied. To verify the FM ground state of $MnBi_2Te_4$, we perform DFT + U and DFT + U + SOC (where SOC represents "spin-orbit coupling") calculations to obtain the total energies of three magnetic configurations, i.e., FM, AFM-I, and AFM-II shown in Fig. 1(b) (for details of our computations, see Sec. I of the Supplemental Material (SM) [35]). The energies per formula unit of the AFM-I and AFM-II states relative to that of the FM state are summarized in Fig. 1(b). In the absence and presence of SOC in the calculations, the relative energy of AFM-I is 2.42 and 4.52 meV, respectively, and that of AFM-II is 3.06 and 4.48 meV, respectively. Furthermore, our calculations show that the magnetic anisotropy energy is negligible compared with the exchange energy (see Sec. IV of the SM [35]). That is, regardless of whether the SOC is included or not, the ground state is always FM. Hence, it is reasonable to ignore SOC in our discussion (we will discuss briefly the effect of SOC later). Using the four-states method [38,51], we evaluate the first-, second-, and third-nearest-neighbor (NN) spin exchanges J_1, J_2, and J_3, respectively, to find that J_1 is FM (−0.94 meV), J_2 is AFM (0.14 meV), and J_3 is FM (−0.038 meV). J_3 is one and two orders of magnitude smaller than J_1 and J_2, respectively, and can be ignored. Because the first and second NN spin exchanges are opposite in sign, one might consider the possibility of a noncollinear spin arrangement, such as a spiral order for $MnBi_2Te_4$. We examined this possibility by carrying out the Freiser analysis [40] (for details, see Sec. II and Fig. S1(a) of the SM [35]) and Monte Carlo simulation [39] (for details, see Sec. III and Fig. S1(b) of the SM [35]), to find that the ground state of $MnBi_2Te_4$ is, indeed, FM. We note that the Mn atoms of MnTe [52] and $MnBi_2Te_4$ have the same oxidation state, and the $MnTe_6$ octahedral environments are similar in these two compounds. MnTe has an A-type antiferromagnetic structure with ferromagnetic arrangement of the magnetic moments on the ab plane. However, we find that this in-plane ferromagnetic alignment arises from the competition among the nearest-, next-nearest-, and next-next-nearest-neighbor exchange interactions rather than from violating the Goodenough-Kanamori rules (for details, see Sec. VII of the SM [35]).

The crystal structure and the band dispersion relations of $MnBi_2Te_4$ are presented in Fig. S2 of the SM [35], and the partial density of states (PDOS) plots in Fig. S3 of the SM [35]. The latter manifest that: (1) The occupied d states of Mn, occurring approximately 4 eV below the Fermi level (0 eV), form a very narrow band. (2) In the occupied energy region between approximately −4 eV and the Fermi level, the p states of both Te and Bi occur and overlap significantly, suggesting that there exists a strong hybridization between Te $5p$ and Bi $6p$ states. (3) We find that the major component of the valence-band maximum is the Te p orbitals and that

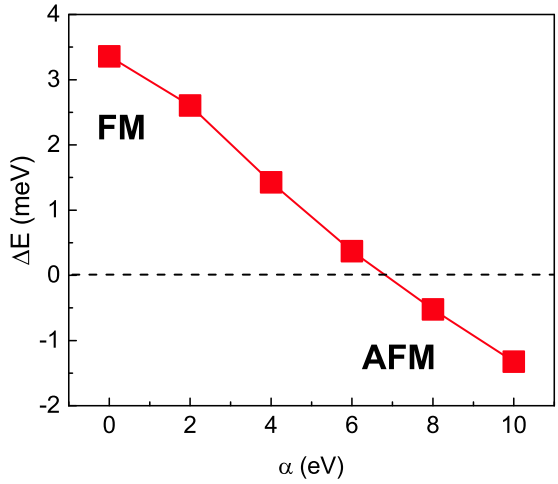

FIG. 2. The exchange energy $\Delta_{ex} = E_{AFM} - E_{FM}$ as a function of α, where α is the tunable parameters positively correlated with the energy shift of the Bi $6p$ orbitals.

of the conduction-band minimum is the Bi p orbitals and that there is a strong hybridization between Bi p and Te p orbitals. Thus, one might speculate if the hybridization of Bi $6p$ orbitals with the $5p$ orbitals of the inner Te forming the first coordinate of the Mn^{2+} cations is responsible for the FM coupling between the Mn^{2+} cations. One way to test this speculation is to perform calculations for a hypothetical layer system of Mn^{2+} ions that may simulate the $MnTe_2$ layer of $MnBi_2Te_4$ without Bi atoms. Such a system is the "MnI_2" layer that has the structure of the $MnTe_2$ layer of $MnBi_2Te_4$ (see Fig. S4 of the SM [35]). Our calculations for this model system reveal that the AFM-I state is more stable than the FM state (by 0.41 meV per formula unit), suggesting that the Bi atoms are important for the FM coupling in $MnBi_2Te_4$. Nevertheless, MnI_2 is different in structure from the $MnTe_2$ layer of $MnBi_2Te_4$. Thus, we perform calculations for $MnBi_2Te_4$ by raising only the energy of the Bi $6p$ orbital using the orbital selective external potential method so as to weaken the hybridization between the Bi $6p$ and Te $5p$ orbitals [53,54]. Figure 2 shows that, with raising the energy level of the Bi $6p$ orbital, the energy difference $\Delta E = E_{AFM} - E_{FM}$ decreases almost linearly so that the AFM state becomes more stable than the FM state when the energy of the Bi $6p$ orbital is raised more than a critical value (approximately 2 eV). It should be pointed out that the energy scale of Fig. 2 does not mean the real shift of the Bi p orbitals but refers to the tunable parameter α in the modified VASP. The latter increases with increasing the shift of the Bi p orbitals (for details, see Sec. VI of the SM [35]). This result once again shows that the Bi ion is necessary for the FM coupling in $MnBi_2Te_4$. A primary consequence of the hybridization between the Bi $6p$ orbitals and the $5p$ orbitals of the inner Te is that some electron density of the inner Te^{2-} anions is transferred to the Bi^{3+} cations. If this electron transfer is essential for the FM coupling between the Mn^{2+} ions, the amount of this electron transfer should be greater in the FM than in the AFM state. As shown in Sec. VIII of the SM [35], this is, indeed, the case and the energy lowering associated with the electron transfer from the inner Te^{2-} ions toward the Bi^{3+} cations is greater in the FM state than in the AFM state.

To thoroughly understand the mechanism of the FM coupling in $MnBi_2Te_4$, we carry out a model Hamiltonian analysis. First, we consider a three-site cluster (TM-L-TM) model composed of two TM atoms bridged by an L atom, shown as the inset in the left panel of Fig. 3. In the case of $MnBi_2Te_4$, TM and L represent the Mn and Te atoms, respectively. For simplicity, we consider a single orbital for each atom. There are four electrons, i.e., one for each TM atom and two for the L atom. Here, we adopt a TB method based on the mean-field approximation [43,47] to obtain the exchange energy $\Delta_{ex} = E_{AFM} - E_{FM}$. We consider only the hopping (t) between the p orbital of L and the d orbital of the TM since two transition-metal atoms are far apart. The numerically calculated exchange energy Δ_{ex} was plotted as a function of the hopping parameter t in the left panel of Fig. 3, which indicates that the ground state is AFM. The same conclusion can be reached using the perturbation theory (for details, see Sec. IX of the SM [35]), in agreement with the Goodenough-Kanamori rule.

Now, we consider a four-site cluster [TM-L(M)-TM] model derived from the three-site cluster model by attaching an atom (M) with one empty p orbital to L (shown in the right panel of Fig. 3). In our case, Bi takes the role of atom M. In addition to the hopping t from the p orbital of L to the d orbital of the TM, there exists another hopping t' from the p orbital of M to the p orbital of L. Note that the hybridization between the TM and the M is omitted since they are far apart. At this stage, we discuss the occupied energy in two different magnetic configurations, FM and AFM. (a) FM alignment. Due to the charge balance, the three spin-up electrons must occupy three spin-up orbitals of the two TM atoms and one L atom. In the spin-up manifold, the p-d hopping pushes up the p orbital of L by $2t^2/\Delta_{pd}$. Here, $\Delta_{pd} = \varepsilon_p - \varepsilon_d$ is the on-site energy difference between the d orbital of the TM and the p-orbital of L, which is denoted in Fig. 4(a). Note that, in our case, $\Delta_{pd} > 0$. The introduction of the M atom pushes down the p orbital of L by $\delta^{\uparrow}_{p'p} = \frac{t'^2}{\Delta_{p'p} - 2t^2/\Delta_{pd}}$, where $\Delta_{p'p} = \varepsilon_{p'} - \varepsilon_p$ is the on-site energy difference between the p orbital of M and that of L. To keep the orbital of the M atom mostly empty, we require $\frac{\Delta_{p'p}\Delta_{pd}}{t^2} > 2$. For the spin-down manifold, we performed a similar analysis by noting that the p orbital of L is pushed down by $2t^2/(U - \Delta_{pd})$. Here, U is the on-site repulsion of the TM atom, which is denoted in Fig. 4. By introducing the surrounding atom M, the p-p hopping pushes down the p orbital of L by $\delta^{\downarrow}_{p'p} = \frac{t'^2}{\Delta_{p'p} + 2t^2/(U - \Delta_{pd})}$ as shown in Fig. 4(b). Note that the spin-down electron occupies the p orbital of L. The total energy gain for the FM alignment due to the introduction of M is given by $\Delta E_{FM} = \delta^{\uparrow}_{p'p} + \delta^{\downarrow}_{p'p}$. (b) AFM alignment. In this case, two spin-up electrons occupy the d orbital of the left TM and the p orbital of L, whereas two spin-down electrons occupy the d orbital of the right TM and the p orbital of L. We first consider the spin-up manifold without atom M. Then, the high-energy empty d orbital of the TM hybridizes with the p orbital of L to push the latter by $t^2/(U - \Delta_{pd})$. The hybridization between the two occupied orbitals also pushes up the p orbital of L by t^2/Δ_{pd}. Hence,

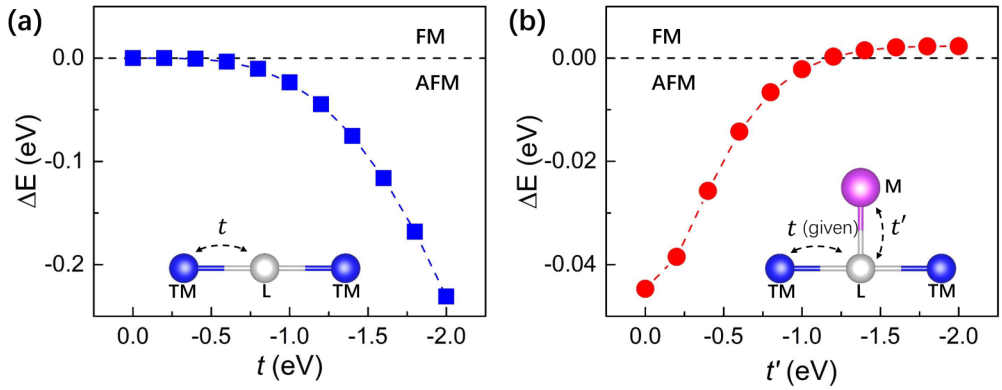

FIG. 3. The exchange energies obtained for the three-site and four-site cluster models. The left panel shows the exchange energy of the three-site cluster model (inset) as a function of the hopping parameter t. The right panel shows the exchange energy of the four-site cluster model as a function of the hopping parameter t' with the hopping t fixed to a reasonable value (−1.2 eV). In both cases, the on-site energy is set according to the PDOS of $MnBi_2Te_4$.

the p orbital of L shifts by $t^2/\Delta_{pd} - t^2/(U - \Delta_{pd})$. Now, we include the influence of atom M. The p-p hopping between the p orbitals of M and L pushes down the p orbital of L by $\delta^{\uparrow}_{p'p} = \frac{t'^2}{\Delta_{p'p} - t^2/\Delta_{pd} + t^2/(U-\Delta_{pd})}$ as shown in Fig. 4(b). For the spin-down manifold, the energy gain is same as the spin-up manifold. Therefore, the total energy gain due to the introduction of M is given by $\Delta E_{AFM} = 2\delta^{\uparrow}_{p'p}$. Comparing the energy gains in the FM and AFM states caused by introducing the surrounding atom M, we obtain $\Delta E_{\text{gain}} = \Delta E_{FM} - \Delta E_{AFM}$,

$$\Delta E_{\text{gain}} = \frac{2\alpha^2 t'^2 \Delta_{pd}}{t^2(\beta-2)[(\alpha-1)\beta+2][(\alpha-1)(\beta-1)+1]},$$

where $\alpha = \frac{U}{\Delta_{pd}} > 1$ in order to keep the L orbital occupied and $\beta = \frac{\Delta_{p'p}\Delta_{pd}}{t^2} > 2$ as mentioned before. Therefore, ΔE_{gain} is always larger than 0, so the energy gain of the FM state is greater than that of the AFM alignment. This mechanism can also be intuitively seen from Figs. 4(a) and 4(c). In the FM state, the p-p hybridization is stronger than that in AFM, which results in a greater lowering of the p orbital of L. The difference in the different energy gains is proportional to the square of the p-p hopping t'. Therefore, the ground state of the system depends on the competition between the different energy gains ΔE_{gain} and the exchange energy Δ_{ex} of the three-site cluster. The stronger the p-p hopping, the more likely it is to achieve the FM ground state. In Fig. 3(b), we plot the numerically computed exchange energy as a function of the p-p hopping t' to find that an AFM-to-FM transition can, indeed, occur when $|t'|$ is increasing.

As discussed above and in Sec. IX of the SM [35], each Bi^{3+} cation attached to the inner Te^{2-} anion forming the

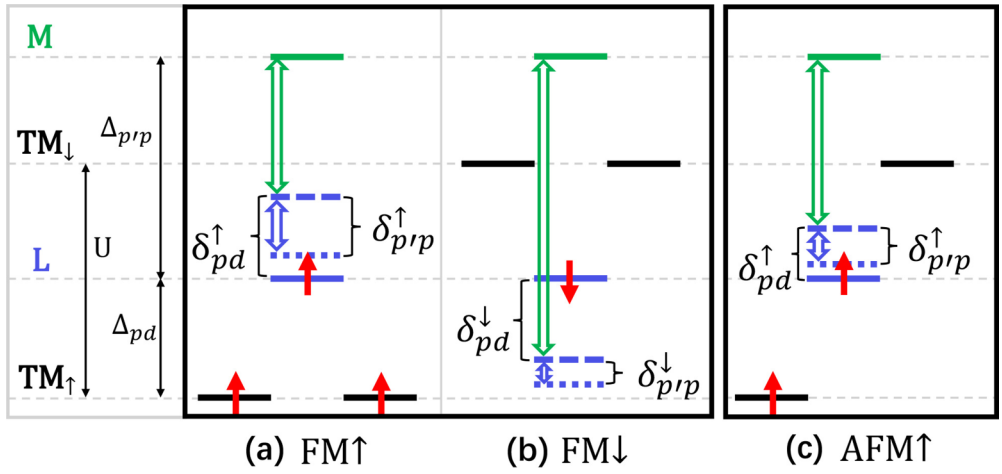

FIG. 4. Schematic for the FM mechanism in $MnBi_2Te_4$. (a) and (b) show the up-spin and down-spin energy levels in the case of FM coupling between the two TM ions, respectively. (c) illustrates the up-spin energy levels in the case of AFM coupling between the two TM ions (the down-spin levels are the same as the up-spin case). The blue dashed lines refer to the ligand levels after the p-d hybridization between the TM and the L atoms, and the blue solid lines represent the ligand levels after the p-p hybridization between the L and the M atoms. The green hollow double-headed arrows mark the energy difference between the L and the M atoms after the p-d hybridization. The blue hollow double-headed arrows represent the energy gained from the p-p hybridization, and the red arrows represent the electron with a definite spin state.

Mn-Te-Mn superexchange path is crucial for the FM coupling between the Mn^{2+} magnetic ions. Additionally, as mentioned earlier, SOC enhances ferromagnetism. Comparing the PDOS without and with SOC (see Sec. V of the SM [35]), we find that the Bi $6p$ orbital is lowered in energy under SOC. The latter will enhance the p-p hybridization between the p orbitals of M and L, resulting in a stronger FM coupling between the two TMs. This conclusion is consistent with our four-sites model.

To summarize, the origin of the FM coupling in $MnBi_2Te_4$ was explored in three steps. First, we confirmed the FM state is the ground state of a $MnBi_2Te_4$ monolayer through DFT calculations. Then, we found that the Bi^{3+} cation attached to the inner Te^{2-} anion forming the Mn-Te-Mn superexchange path plays a crucial role for the FM coupling between the adjacent Mn^{2+} cations through performing test DFT calculations. Finally, using a model TB Hamiltonian, it was shown why the hybridization of the Bi $6p$ orbital with the $5p$ orbital of the inner Te makes the FM coupling more favorable energetically than the AFM coupling. The mechanism of the FM coupling in $MnBi_2Te_4$ revealed in this Rapid Communication is fundamentally different from that in CrI_3 and $CrGeTe_3$ where the coupling between the occupied t_{2g} orbital and the empty e_g orbital is the key.

This work was supported by NSFC (Grant No. 11825403), the Program for Professor of Special Appointment (Eastern Scholar), Qing Nian Ba Jian Program. J.S.F. acknowledges support from the Anhui Provincial Natural Science Foundation (Grant No. 1908085MA10). H.-J.K. acknowledges support from the Basic Sciences Research Program through the National Research Foundation of Korea (NRF) funded by the Ministry of Education (Grant No. NRF-2017R1D1A1B03029624). H.J.X. thanks Dr. J. Wang for useful discussions.

[1] M. Z. Hasan and C. L. Kane, Rev. Mod. Phys. **82**, 3045 (2010).
[2] X.-L. Qi and S.-C. Zhang, Rev. Mod. Phys. **83**, 1057 (2011).
[3] B. A. Bernevig, T. L. Hughes, and S.-C. Zhang, Science **314**, 1757 (2006).
[4] R. Yu, W. Zhang, H.-J. Zhang, S.-C. Zhang, X. Dai, and Z. Fang, Science **329**, 61 (2010).
[5] H. Pan, Z. Li, C.-C. Liu, G. Zhu, Z. Qiao, and Y. Yao, Phys. Rev. Lett. **112**, 106802 (2014).
[6] Z. F. Wang, Z. Liu, and F. Liu, Phys. Rev. Lett. **110**, 196801 (2013).
[7] H. Zhang, C. Lazo, S. Blügel, S. Heinze, and Y. Mokrousov, Phys. Rev. Lett. **108**, 056802 (2012).
[8] Z. Qiao, W. Ren, H. Chen, L. Bellaiche, Z. Zhang, A. H. MacDonald, and Q. Niu, Phys. Rev. Lett. **112**, 116404 (2014).
[9] J. Wang, B. Lian, and S.-C. Zhang, Phys. Scr. **2015**, 014003 (2015).
[10] C.-Z. Chang, J. Zhang, X. Feng, J. Shen, Z. Zhang, M. Guo, K. Li, Y. Ou, P. Wei, and L.-L. Wang, Science **340**, 167 (2013).
[11] Q. L. He, X. Kou, A. J. Grutter, G. Yin, L. Pan, X. Che, Y. Liu, T. Nie, B. Zhang, and S. M. Disseler, Nature Mater. **16**, 94 (2017).
[12] M. Mogi, M. Kawamura, R. Yoshimi, A. Tsukazaki, Y. Kozuka, N. Shirakawa, K. Takahashi, M. Kawasaki, and Y. Tokura, Nature Mater. **16**, 516 (2017).
[13] L. A. Wray, S.-Y. Xu, Y. Xia, D. Hsieh, A. V. Fedorov, Y. San Hor, R. J. Cava, A. Bansil, H. Lin, and M. Z. Hasan, Nat. Phys. **7**, 32 (2011).
[14] D. Xiao, J. Jiang, J.-H. Shin, W. Wang, F. Wang, Y.-F. Zhao, C. Liu, W. Wu, M. H. W. Chan, N. Samarth, and C.-Z. Chang, Phys. Rev. Lett. **120**, 056801 (2018).
[15] E. Rienks, S. Wimmer, J. Sánchez-Barriga, O. Caha, P. Mandal, J. Růžička, A. Ney, H. Steiner, V. Volobuev, and H. Groiss, Nature (London) **576**, 423 (2019).
[16] D. Zhang, M. Shi, T. Zhu, D. Xing, H. Zhang, and J. Wang, Phys. Rev. Lett. **122**, 206401 (2019).
[17] J. Li, Y. Li, S. Du, Z. Wang, B.-L. Gu, S.-C. Zhang, K. He, W. Duan, and Y. Xu, Sci. Adv. **5**, eaaw5685 (2019).
[18] Y. Deng, Y. Yu, M. Z. Shi, Z. Guo, Z. Xu, J. Wang, X. H. Chen, and Y. Zhang, Science **367**, 895 (2020).
[19] Y. Gong, J. Guo, J. Li, K. Zhu, M. Liao, X. Liu, Q. Zhang, L. Gu, L. Tang, and X. Feng, Chin. Phys. Lett. **36**, 076801 (2019).
[20] M. Otrokov, I. Klimovskikh, H. Bentmann, D. Estyunin, A. Zeugner, Z. Aliev, S. Gaß, A. Wolter, A. Koroleva, and A. Shikin, Nature (London) **576**, 416 (2019).
[21] R. S. K. Mong, A. M. Essin, and J. E. Moore, Phys. Rev. B **81**, 245209 (2010).
[22] X.-L. Qi, T. L. Hughes, and S.-C. Zhang, Phys. Rev. B **78**, 195424 (2008).
[23] A. M. Essin, J. E. Moore, and D. Vanderbilt, Phys. Rev. Lett. **102**, 146805 (2009).
[24] F. Wilczek, Phys. Rev. Lett. **58**, 1799 (1987).
[25] C. Gong, L. Li, Z. Li, H. Ji, A. Stern, Y. Xia, T. Cao, W. Bao, C. Wang, and Y. Wang, Nature (London) **546**, 265 (2017).
[26] B. Huang, G. Clark, E. Navarro-Moratalla, D. R. Klein, R. Cheng, K. L. Seyler, D. Zhong, E. Schmidgall, M. A. McGuire, and D. H. Cobden, Nature (London) **546**, 270 (2017).
[27] J. B. Goodenough, *Magnetism and Chemical Bond* (Interscience, New York, 1963), Vol. 1.
[28] J. Kanamori, J. Phys. Chem. Solids **10**, 87 (1959).
[29] P. Anderson, Phys. Rev. **79**, 350 (1950).
[30] J. Kanamori, Prog. Theor. Phys. **17**, 177 (1957).
[31] J. B. Goodenough and A. L. Loeb, Phys. Rev. **98**, 391 (1955).
[32] J.-Q. Yan, Q. Zhang, T. Heitmann, Z. Huang, K. Y. Chen, J.-G. Cheng, W. Wu, D. Vaknin, B. C. Sales, and R. J. McQueeney, Phys. Rev. Mater. **3**, 064202 (2019).
[33] A. M. Oleś, P. Horsch, L. F. Feiner, and G. Khaliullin, Phys. Rev. Lett. **96**, 147205 (2006).
[34] J. Kim, S.-H. Jhi, A. H. MacDonald, and R. Wu, Phys. Rev. B **96**, 140410(R) (2017).
[35] See Supplemental Material at https://link.aps.org/supplemental/10.1103/PhysRevB.101.201408 for details, which include Refs. [36–50] for computation details, supplementary analysis of the electronic structure, and a brief derivation of the tight-binding (TB) model for monolayer $MnBi_2Te_4$.
[36] G. Kresse and J. Furthmüller, Comput. Mater. Sci. **6**, 15 (1996).
[37] Y. Li, Z. Jiang, J. Li, S. Xu, and W. Duan, Phys. Rev. B **100**, 134438 (2019).

[38] H. Xiang, C. Lee, H.-J. Koo, X. Gong, and M.-H. Whangbo, Dalton Trans. **42**, 823 (2013).
[39] Y. Miyatake, M. Yamamoto, J. Kim, M. Toyonaga, and O. Nagai, J. Phys. C: Solid State Phys. **19**, 2539 (1986).
[40] M. Freiser, Phys. Rev. **123**, 2003 (1961).
[41] P. E. Blöchl, Phys. Rev. B **50**, 17953 (1994).
[42] S. L. Dudarev, G. A. Botton, S. Y. Savrasov, C. J. Humphreys, and A. P. Sutton, Phys. Rev. B **57**, 1505 (1998).
[43] J. S. Feng and H. J. Xiang, Phys. Rev. B **93**, 174416 (2016).
[44] G. Kresse and J. Furthmüller, Phys. Rev. B **54**, 11169 (1996).
[45] G. Kresse and D. Joubert, Phys. Rev. B **59**, 1758 (1999).
[46] H. J. Monkhorst and J. D. Pack, Phys. Rev. B **13**, 5188 (1976).
[47] H. Katsura, N. Nagaosa, and A. V. Balatsky, Phys. Rev. Lett. **95**, 057205 (2005).
[48] J. P. Perdew, K. Burke, and M. Ernzerhof, Phys. Rev. Lett. **77**, 3865 (1996).
[49] P. S. Wang, W. Ren, L. Bellaiche, and H. J. Xiang, Phys. Rev. Lett. **114**, 147204 (2015).
[50] R. Winkler, Springer Tracts Mod. Phys. **191**, 1 (2003).
[51] H. J. Xiang, E. J. Kan, S.-H. Wei, M.-H. Whangbo, and X. G. Gong, Phys. Rev. B **84**, 224429 (2011).
[52] D. Kriegner, H. Reichlova, J. Grenzer, W. Schmidt, E. Ressouche, J. Godinho, T. Wagner, S. Y. Martin, A. B. Shick, V. V. Volobuev, G. Springholz, V. Holý, J. Wunderlich, T. Jungwirth, and K. Výborný, Phys. Rev. B **96**, 214418 (2017).
[53] X. Wan, J. Zhou, and J. Dong, Europhys. Lett. **92**, 57007 (2010).
[54] Y. Du, H.-C. Ding, L. Sheng, S. Y. Savrasov, X. Wan, and C.-G. Duan, J. Phys.: Condens. Matter **26**, 025503 (2013).